Table S1. Allele frequency, QC index, and Q value of the candidate SNPs

	Stage 1				Stage 2				
dbSNP ID	Allele frequency case	Allele frequency control	HWE* control	Call rate†	Allele frequency case	Allele frequency control	HWE* control	Call rate†	Q value‡
rs547984	0.55	0.46	0.0496	1.00	0.52	0.46	0.786	1.00	0.28
rs540782	0.56	0.46	0.0269	1.00	0.52	0.46	0.786	1.00	0.22
rs693421	0.55	0.45	0.0433	0.99	0.51	0.46	0.901	1.00	0.30
rs2499601	0.55	0.46	0.0635	1.00	0.51	0.46	0.741	1.00	0.25
rs7081455	0.83	0.74	0.8475	0.99	0.82	0.78	0.560	1.00	0.22
rs7961953	0.34	0.26	0.5426	1.00	0.32	0.27	0.004	1.00	0.45

Allele frequency was higher in case samples than in control samples.
*HWE, *P* value for the deviation from HWE.
†Call rate, call rate per SNP in case plus control samples.
‡Q value, index for quantifying heterogeneity between stages 1 and 2, expressed as a *P* value.

Table S2. Calculation of AIC by logistic regression analysis in various genetic models

	Genetic model	Combination of SNPs			AIC	AIC difference*
One-factor	Additive	rs547984			2166.4	8.8
		rs7081455			2157.6	0.0‡
		rs7961953			2167.5	9.9
	Genotype†	rs547984			2167.1	9.5
		rs7081455			2159.5	1.9
		rs7961953			2168.6	11.0
	Dominant/recessive	rs547984			2167.0	9.4
		rs7081455			2159.0	1.4
		rs7961953			2167.3	9.7
Two-factor	Additive	rs547984	rs7081455		2142.1	0.8
		rs7081455	rs7961953		2141.3	0.0‡
		rs547984	rs7961953		2151.5	10.2
	Genotype†	rs547984	rs7081455		2144.1	2.8
		rs7081455	rs7961953		2144.8	3.5
		rs547984	rs7961953		2153.5	12.2
	Dominant/recessive	rs547984	rs7081455		2143.2	1.9
		rs7081455	rs7961953		2143.9	2.6
		rs547984	rs7961953		2152.8	11.5
Two-factor interaction	Additive	rs547984	rs7081455		2143.2	1.9
		rs7081455	rs7961953		2143.2	1.9
		rs547984	rs7961953		2153.0	11.7
	Genotype†	rs547984	rs7081455		2150.1	8.8
		rs7081455	rs7961953		2150.2	8.9
		rs547984	rs7961953		2159.0	17.7
	Dominant/recessive	rs547984	rs7081455		2144.3	3.0
		rs7081455	rs7961953		2145.6	4.3
		rs547984	rs7961953		2153.5	12.2
Three-factor	Additive	rs547984	rs7081455	rs7961953	2124.9	0.0‡
	Genotype†	rs547984	rs7081455	rs7961953	2128.8	3.9
	Dominant/recessive	rs547984	rs7081455	rs7961953	2128.1	3.2
Three-factor interaction	Additive	rs547984	rs7081455	rs7961953	2130.1	5.2
	Genotype†	rs547984	rs7081455	rs7961953	2144.8	19.9
	Dominant/recessive	rs547984	rs7081455	rs7961953	2132.1	7.2

*AIC difference, difference from the AIC of the best-fitting model.
†Genotype model, classification variable of 3 genotypes: *AA*, *AB*, and *BB*.
‡Best fit model of AIC difference is supposed to be 0.

Table S3. Summary of AIC in an additive model without interaction

	Combination of SNPs			AIC	AIC difference*
One-factor	rs547984			2166.4	41.5
	rs7081455			2157.6	33.0
	rs7961953			2167.5	42.6
Two-factor	rs547984	rs7081455		2142.1	17.2
	rs7081455	rs7961953		2141.3	16.4
	rs547984	rs7961953		2151.5	26.6
Three-factor	rs547984	rs7081455	rs7961953	2124.9	0.0†

*AIC difference, difference from the AIC of the best-fitting model.
†Best-fit model of the AIC difference is supposed to be 0.

Table S4. Clinical characteristics of case and control subjects in stage 1 plus 2 populations

	Case	Control	*P* value
No. subjects in combined analyses	827	748	
Female/male ratio	1.02 (827)	1.58 (748)	<0.05*
Age (years)† at:			
Blood sampling	63.3 ± 13.7 (827)	53.6 ± 14.5‡ (748)	<0.05§
Diagnosis	57.1 ± 13.7 (625)	53.6 ± 14.5‡ (748)	<0.05§
Medical history,¶			
Neurovascular disorder, %	2.6	0.4	<0.05*
Cardiovascular disorder, %	12.1	6.5	<0.05*
Diabetes mellitus, %	9.3	3.8	<0.05*
Hyperlipidemia, %	10.3	11.0	0.69*
Hypertension, %	22.1	15.5	<0.05*
Headache, %	12.5	13.8	0.47*
Peripheral circulatory disorder, %	56.5	64.1	<0.05*
Thyroid disorder, %	2.6	1.3	0.09*

Numbers in the parentheses are the total numbers of samples used for analysis.
*P value analyzed by χ^2 test between case and control data.
†All the data are shown as mean ± SD.
‡Age at time of blood sampling and diagnosis is the same for the control samples.
§P value analyzed by Student's t test between case and control data.
¶Data were obtained from 745 case patients and 682 control subjects.

Table S5. Analysis of confounding effects of age, sex, and medical histories for the candidate SNPs in stage 1 plus 2 population

dbSNP ID	Status	Age at blood sampling*	Age at diagnosis†	Sex‡	Neurovascular disorder‡	Cardiovascular disorder‡	Diabetes mellitus‡	Hyper-tension‡	Peripheral circulatory disorder‡
rs547984	Case	0.59	0.16	0.28	0.98	0.26	<0.05	0.74	0.62
	Control	0.15	0.15	0.66	0.32	0.61	0.29	0.70	0.20
rs540782	Case	0.55	0.11	0.30	0.98	0.27	<0.05	0.74	0.61
	Control	0.13	0.13	0.65	0.32	0.63	0.30	0.73	0.25
rs693421	Case	0.57	0.12	0.33	0.99	0.34	<0.05	0.72	0.60
	Control	0.06	0.06	0.83	0.33	0.73	0.30	0.77	0.20
rs2499601	Case	0.82	0.33	0.28	0.99	0.34	<0.05	0.59	0.56
	Control	0.08	0.08	0.79	0.32	0.58	0.29	0.65	0.28
rs7081455	Case	0.43	0.60	0.99	0.66	0.72	0.94	0.66	0.94
	Control	0.82	0.82	0.06	0.14	0.20	0.30	0.61	0.64
rs7961953	Case	0.52	0.29	0.98	0.20	0.74	0.20	0.97	0.18
	Control	0.70	0.70	0.71	0.86	0.52	0.27	0.68	0.52

Note that the age at the blood sampling and diagnosis are the same in the control samples and have the same *P* values.
*Data show the *P* value analyzed by one-way ANOVA for 827 case and 748 control subjects.
†Data show the *P* value analyzed by one-way ANOVA in 625 case and 748 control subjects.
‡All data show the *P* value analyzed by χ^2 test for 745 case and 682 control subjects.

LETTER

Lack of association of three primary open-angle glaucoma-susceptible loci with primary glaucomas in an Indian population

Nakano et al. (1) demonstrated significant association of six single nucleotide polymorphisms (SNPs) with primary open-angle glaucoma (POAG) that flanked genes on chromosomes 1 (*ZP4*), 10 (*PLXDC2*), and 12 (*DKFZp762A217*) in a Japanese population. The associations were consistent based on a two-stage genome-wide association study (GWAS) design, despite a mixture of both classical POAG [with raised intraocular pressure (IOP)] and normal-tension glaucoma (NTG) in their cohort. Genetic associations are biologically more meaningful if they are replicated across different ethnic groups (2). We tried to replicate these findings in 470 subjects from another Asian population (Indian) that included cases of POAG (n = 140) and ethnically matched normal controls (n = 219). A cohort of primary angle-closure glaucoma (PACG; n = 111) was also included to see whether these variations were also involved in another form of primary glaucoma. The regions harboring these SNPs were screened by resequencing and the variants further validated by restriction digestion.

There was no significant association to any of these six SNPs with POAG and PACG in our cohort (Table 1). Several explanations could be provided to account for this difference in the results between the two studies: (*i*) we enrolled cases of POAG and PACG based on a stringent inclusion criteria (3) and all of the patients had raised IOP unlike the Japanese cohort that had a mixture of both high- and low-pressure glaucomas; (*ii*) the differences in the allele frequency did not exceed 5% (except for rs2499601) between our POAG cases and controls (Table 1) compared to the stage I cohort in the previous study; (*iii*) the allele frequencies among the normal controls in two Japanese cohorts were much higher at all of the six loci compared to the normal controls from India, indicating perhaps a different genetic profile; (*iv*) the lack of association was unlikely due to the effect of population structuring as evident from a similar allele and haplotype frequencies among the patients (Table 1) of two different glaucoma phenotypes (POAG and PACG) enrolled from the same ethnic and geographic backgrounds from Southern India; and, lastly, (*v*) these differences would be unlikely due to experimental errors because the screening was undertaken by resequencing. We also observed other rare variants flanking these candidate SNPs in these regions (minor allele frequency, <0.5) and have not included them in the analysis. The four SNPs in chromosome 1 indicated strong linkage disequilibrium between them (D′ = 0.90–1.0), but haplotypes generated with these did not indicate any association with POAG and PACG (Table 1).

We conclude that the association of these six candidate SNPs is not a universal phenomenon. Unlike significant associations observed with *LOXL1* SNPs in exfoliation syndrome and exfoliation glaucoma worldwide (4) including Japanese populations (5), these POAG-associated variants need further validation across different populations. It is unlikely that these variants may be associated with IOP-related primary glaucomas.

Kollu N. Rao, Inderjeet Kaur, and Subhabrata Chakrabarti[1]
Brien Holden Eye Research Centre, L. V. Prasad Eye Institute, Hyderabad 500034, India

1. Nakano M, et al. (2009) Three susceptible loci associated with primary open-angle glaucoma identified by genome-wide association study in a Japanese population. *Proc Natl Acad Sci USA* 106:12838–12842.
2. Chanock SJ, et al. (2007) Replicating genotype-phenotype associations. *Nature* 447:655–660.
3. Chakrabarti S, et al. (2007) Glaucoma-associated *CYP1B1* mutations share similar haplotype backgrounds in POAG and PACG phenotypes. *Invest Ophthalmol Vis Sci* 48:5439–5444.
4. Challa P (2009) Genetics of pseudoexfoliation syndrome. *Curr Opin Ophthalmol* 20:88–91.
5. Tanito M, et al. (2008) LOXL1 variants in elderly Japanese patients with exfoliation syndrome/glaucoma, primary open-angle glaucoma, normal tension glaucoma, and cataract. *Mol Vis* 14:1898–905.

Author contributions: I.K. and S.C. designed research; K.N.R. and I.K. performed research; S.C. analyzed data; and S.C. wrote the paper.

The authors declare no conflict of interest.

[1]To whom correspondence should be addressed at: Kallam Anji Reddy Molecular Genetics Laboratory, Brien Holden Eye Research Centre, L. V. Prasad Eye Institute, Hyderabad 500034, India. E-mail: subho@lvpei.org.

Table 1. Distribution of allele and haplotype frequencies in POAG and PACG cases and normal controls in an Indian population

	Associated allele	Frequency in POAG cases	Frequency in controls	*P* value*	Frequency in PACG cases	Frequency in controls	*P* value*
SNPs							
rs547984	A	0.417	0.363	0.437	0.441	0.363	0.271
rs540782	C	0.409	0.356	0.443	0.436	0.356	0.255
rs693421	T	0.405	0.357	0.616	0.444	0.357	0.190
rs2499601	C	0.482	0.413	0.286	0.505	0.413	0.168
rs7081455	G	0.424	0.407	0.629	0.390	0.407	0.676
rs7961953	G	0.814	0.778	0.251	0.830	0.778	0.124
Haplotypes†							
C-G-G-T		0.485	0.564	0.143	0.466	0.564	0.130
A-C-T-C		0.383	0.332	0.523	0.403	0.332	0.354
C-G-G-C		0.088	0.058	0.376	0.051	0.058	0.999
C-G-T-C		0.007	0.012	0.999	0.015	0.012	0.999

*Permutation *P* value (based on 10,000 permutations).

†Haplotypes based on the four chromosome 1 SNPs. The estimated haplotype frequencies were calculated with the Haploview software (ver 4.0). The order of the haplotype is rs547984-rs540782-rs693421-rs2499601.

Reply to Rao et al.: Appropriate study design for genome-wide association study replication to identify variants modestly associated with complex traits

We sincerely thank Rao et al. (1) for their remarks about our recently published article (2). Rao et al. (1) attempted to replicate our results of primary open-angle glaucoma (POAG)-associated SNPs identified in Japanese (2) by using an Indian population. This is an important trial, because it was conducted in order to see whether POAG shared the same variants across different ethnic backgrounds. It is also quite important to properly assess the data from multiple sites in order to gain statistical power and identify latent variants associated with complex traits, especially when no major risk gene or locus was observed in the initial genome-wide association study (GWAS). Unlike the SNPs on the genes strongly associated with age-related macular degeneration (AMD) (3), we could not identify such SNPs in POAG that reached the genome-wide significant threshold (2). This is probably due to the fact that glaucoma seems to have more heterogeneous phenotypes than AMD and multiple gene–gene and gene–environment interactions, each with a small effect, thereby possibly playing critical roles in the onset of the disease. Therefore, we concluded that the discovered SNPs were "modestly" associated and would provide a foundation on which to build (2).

In order to identify disease-associated variants with relatively small effects and draw a conclusion as to whether the results were replicated or not, it is vital that the studies of both the GWAS and its replication are carefully designed. Thus, we paid strict attention to precisely following the GWAS guidelines (4) for our initial GWAS (2). It should be noted that the GWAS guidelines clearly state that a replication study needs to be performed with: (*i*) a sufficient sample size, (*ii*) the same or very similar phenotype, (*iii*) a similar population, and (*iv*) the same study design details. Because Rao et al. (1) aimed at assessing the variants in a different ethnicity, the correlation between the two studies, except for that of point *iii*, should be considered. They performed resequencing and obtained high-quality genotypes from a homogeneous population. They used two distinct subtypes of glaucoma independently: POAG and primary angle-closure glaucoma (PACG), both of which are characterized by patients with high intraocular pressure (IOP). Because many Japanese patients diagnosed with POAG are known to have normal IOP (5), our study may have not detected SNPs related to the control of IOP, as Rao et al. pointed out (1). However, one of the most critical points of the design is the sample size, which determines the sensitivity that is necessary to confirm the replication.

In conclusion, we believe that it is too early to deduce that the association of the six SNPs shown in our study is not a universal phenomenon, as described (1). We propose that, as long as the quality and quantity of the population meet the guideline (4), the ideal way to replicate the results of our findings would be to combine the data from multiple sites by meta-analysis. That approach would probably allow for the discovery of a full set of authentic variants of POAG.

***Masakazu Nakano*[a], *Yoko Ikeda*[b], *Tomohito Yagi*[a], *Kazuhiko Mori*[b], *Shigeru Kinoshita*[b,1], *and Kei Tashiro*[a,1]**

Departments of [a]*Genomic Medical Sciences and* [b]*Ophthalmology, Kyoto Prefectural University of Medicine, Kawaramachi-Hirokoji, Kamigyo-ku, Kyoto 602-8566, Japan*

1. Rao KN, Kaur I, Chakrabarti S (2009) Lack of association of three POAG susceptible loci with primary glaucomas in an Indian population. *Proc Natl Acad Sci USA*, 10.1073/pnas.0910416106.
2. Nakano M, et al. (2009) Three susceptible loci associated with primary open-angle glaucoma identified by genome-wide association study in a Japanese population. *Proc Natl Acad Sci USA* 106:12838–12842.
3. Klein RJ, et al. (2005) Complement factor H polymorphism in age-related macular degeneration. *Science* 308:385–389.
4. Chanock SJ, et al. (2007) Replicating genotype-phenotype associations. *Nature* 447:655–660.
5. Iwase A, et al. (2004). The prevalence of primary open-angle glaucoma in Japanese: The Tajimi Study. *Ophthalmology* 111:1641–1648.

Author contributions: M.N., T.Y., and K.T. analyzed data; and M.N., Y.I., T.Y., K.M., S.K., and K.T. wrote the paper.

The authors declare no conflict of interest.

[1]To whom correspondence may be addressed. E-mail: shigeruk@koto.kpu-m.ac.jp and tashiro@koto.kpu-m.ac.jp.

Identification of a novel HLA-B allele, HLA-B*5904

M. Ueta[1,2], M. Matsushita[3], C. Sotozono[2], S. Kinoshita[2] & K. Tokunaga[4]

1 Research Center for Regenerative Medicine, Faculty of Life and Medical Sciences, Doshisha University, Kyoto, Japan
2 Department of Ophthalmology, Kyoto Prefectural University of Medicine, Kyoto, Japan
3 BioBusiness Development, Wakunaga Pharmaceutical Co., Ltd, Hiroshima, Japan
4 Department of Human Genetics, Graduate School of Medicine, University of Tokyo, Tokyo, Japan

Key words: B*5904; human leukocyte antigen-B; new allele

The new human leukocyte antigen (HLA) class I allele, HLA-B*5904 was identified in Japanese individual. HLA-B*5904 differs from HLA-B*5901 by two non-synonymous nucleotide exchanges at codon 163 (ACG to CTG).

The human leukocyte antigen (HLA)-B locus is one of the most polymorphic regions of the human genome. Its members increase continuously with the development of genotyping technology. Thousand one hundred and nine alleles were found at HLA-B locus up to now. HLA-B*59 is

a small family among HLA-B genes. There are only three members altogether from HLA-B*5901 to B*5903 (1). Here, we report on a novel allele, HLA-B*5904.

The HLA-B*5904 was found in a Japanese patient suffered from Stevens–Johnson syndrome with ocular complications. The sample was determined by the low-to-intermediate resolution kit (HLA-B, WAKFlow HLA typing kit; Wakunaga, Hiroshima, Japan). Typing result was inconclusive with one missing probe, resulting with a clear software interpretation of no match found. Closest possible match was indicated as B*5101 and B*5901. To further analysis of the sample, exons 2 and 3 were sequenced in forward and reverse directions. The sequencing result showed a new HLA-B*59 allele in the sample.

To confirm the presence of a novel allele in the sample, DNA fragment including exons 2 and 3 was cloned into the pT7Blue-2 vector (Merck, Darmstadt, Germany). DNA inserts from the cloned alleles were sequenced using M13F (−20) and T7 primers in both directions. The sequence analysis showed that the new allele differed from B*5901 at positions 559 and 560, codon 163 (ACG to CTG), that change the amino acid from threonine to leucine (Figure 1). The sequence 'CTG' at codon 163 is seen in many other HLA-B groups (B*15, B *35, B*44, B*45, B*46, B*49, B*51, B*52, B*53, B*56, B*57, B*58, and B*78). The HLA-B*5904 might have been arisen by gene-conversion-like event of a short fragment in B*5901 with some allele in these groups as donor. Residue 163 is located at the alpha helix of alpha 2 domain, which is the part of the binding pocket of the HLA class I molecule contributing to the binding properties and specificity of the HLA class I molecule (2). Thus, the new HLA class I allele, HLA-B*5904, may substantially differ in its peptide-binding repertoire from the most common B*5901 allele. The sample was typed as A*0201, 0206; B*5101, B*5904; Cw*0102, 1502; DRB1*0405, 1202; DQB1*0301, 0401.

The nucleotide sequence can be viewed in the DDBJ database under the accession number AB467317. The name HLA-B*5904 has been officially assigned by the World Health Organization (WHO) Nomenclature Committee in November 2008. This follows the agreed policy that, subject to the conditions stated in the most recent Nomenclature report (3), names will be assigned to the new sequences as they are identified. Lists of such new names will be published in the following WHO Nomenclature report.

Correspondence
Masaki Matsushita, PhD
BioBusiness Development

```
                      -20                 -15                 -10                  -5
B5901    ATG CGG GTC ACG GCA CCC CGA ACC CTC CTC CTG CTG CTC TGG GGG GCC CTG GCC CTG ACC GAG ACC TGG GCC G|GC
B5904    *** *** *** *** *** *** *** *** *** *** *** *** *** *** *** *** *** *** *** *** *** *** *** *|--

                    5                  10                  15                  20                  25
B5901    TCC CAC TCC ATG AGG TAT TTC TAC ACC GCC ATG TCC CGG CCC GGC CGC GGG GAG CCC CGC TTC ATC GCA GTG GGC
B5904    --- --- --- --- --- --- --- --- --- --- --- --- --- --- --- --- --- --- --- --- --- --- --- ---

                   30                  35                  40                  45                  50
B5901    TAC GTG GAC GAC ACG CAG TTC GTG AGG TTC GAC AGC GAC GCC GCG AGT CCG AGA GAG GAG CCG CGG GCG CCG TGG
B5904    --- --- --- --- --- --- --- --- --- --- --- --- --- --- --- --- --- --- --- --- --- --- --- ---

                   55                  60                  65                  70                  75
B5901    ATA GAG CAG GAG GGG CCG GAG TAT TGG GAC CGG AAC ACA CAG ATC TTC AAG ACC AAC ACA CAG ACT TAC CGA GAG
B5904    --- --- --- --- --- --- --- --- --- --- --- --- --- --- --- --- --- --- --- --- --- --- --- ---

                   80                  85                  90                  95                 100
B5901    AAC CTG CGG ATC GCG CTC CGC TAC TAC AAC CAG AGC GAG GCC G|GG TCT CAC ACT TGG CAG ACG ATG TAT GGC TGC
B5904    --- --- --- --- --- --- --- --- --- --- --- --- --- --- -|-- --- --- --- --- --- --- --- --- --- ---

                  105                 110                 115                 120                 125
B5901    GAC CTG GGG CCG GAC GGG CGC CTC CTC CGC GGG CAT AAC CAG TTA GCC TAC GAC GGC AAG GAT TAC ATC GCC CTG
B5904    --- --- --- --- --- --- --- --- --- --- --- --- --- --- --- --- --- --- --- --- --- --- --- ---

                  130                 135                 140                 145                 150
B5901    AAC GAG GAC CTG AGC TCC TGG ACC GCG GCG GAC ACC GCG GCT CAG ATC ACC CAG CGC AAG TGG GAG GCG GCC CGT
B5904    --- --- --- --- --- --- --- --- --- --- --- --- --- --- --- --- --- --- --- --- --- --- --- ---

                  155                 160                 165                 170                 175
B5901    GTG GCG GAG CAG CTG AGA GCC TAC CTG GAG GGC ACG TGC GTG GAG TGG CTC CGC AGA TAC CTG GAG AAC GGG AAG
B5904    --- --- --- --- --- --- --- --- --- --- --- CT- --- --- --- --- --- --- --- --- --- --- --- ---
                                          ACG --> CTG
                                          Thr --> Leu
                                              163

                  180                 185                 190                 195                 200
B5901    GAG ACG CTG CAG CGC GCG G|AC CCC CCA AAG ACA CAC GTG ACC CAC CAC CCC ATC TCT GAC CAT GAG GCC ACC CTG
B5904    --- --- --- --- --- --- -|** *** *** *** *** *** *** *** *** *** *** *** *** *** *** *** *** ***
```

Figure 1 Alignment of the nucleotide sequence of exon2 and 3 of the new allele HLA-B*5904 with HLA-B*5901. Dashes indicate identity with the B*5901 sequence. Numbers above correspond with the amino acid position in the mature protein. HLA, human leukocyte antigen.

Wakunaga Pharmaceutical Co., Ltd
1624 Shimokotachi
Koda-cho
Akitakata-shi
Hiroshima 739-1195
Japan
Tel: +81 826 452331
Fax: +81 826 454351
e-mail: matsushita_m@wakunaga.co.jp

doi: 10.1111/j.1399-0039.2009.01228.x

References

1. Robinson J, Waller MJ, Parham P et al. IMGT/HLA and IMGT/MHC: sequence databases for the study of the major histocompatibility complex. *Nucleic Acids Res* 2003: **31**: 311–4.
2. Reche PA, Rainherz EL. Sequence variability analysis of human class I and class II MHC molecules: functional and structural correlates of amino acid polymorphisms. *J Mol Biol* 2003: **331**: 623–41.
3. Marsh SGE, Albert ED, Bodmer WF et al. Nomenclature of factors of the HLA system 2004. *Tissue Antigens* 2005: **65**: 301–69.

THE ANATOMICAL RECORD 292:756–763 (2009)

Characteristic Morphology and Distribution of Bone Marrow Derived Cells in the Cornea

TETSUYA TAKAYAMA,[1]* TERUYOSHI KONDO,[2] MASATOSHI KOBAYASHI,[1] KEISUKE OHTA,[1] YOSHIHIRO ISHIBASHI,[1] TAKAAKI KANEMARU,[3] HIDEKI SHIMAZU,[4] FUMIHIKO ISHIKAWA,[5] TAKAHIRO NAKAMURA,[6] SHIGERU KINOSHITA,[6] AND KEI-ICHIRO NAKAMURA[1]

[1]Division of Microscopic and Developmental Anatomy, Department of Anatomy, Kurume University School of Medicine, Kurume, Fukuoka, Japan
[2]Department of Clinical Engineering, School of Health Science, Kyushu University of Health and Welfare, Nobeoka, Miyazaki, Japan
[3]Morphology Core Unit, Kyushu University Hospital, Fukuoka, Japan
[4]Department of Cardiology, Fukuoka Higashi Medical Center, Fukuoka, Japan
[5]Research Unit for Human Disease Model, Rikagaku Kenkyusho (RIKEN) Center for Allergy and Immunology, Yokohama, Japan
[6]Department of Ophthalmology, Kyoto Prefectural University of Medicine, Kyoto, Japan

ABSTRACT

Enhanced green fluorescence protein (eGFP)-labeled bone marrow (BM) cells were transplanted into syngeneic C57BL/6 (wild-type) mice to investigate the distribution pattern, immunohistochemical characteristics, three-dimensional structure, and ultrastructure of the BM-derived cells in the mouse cornea using a fluorescence microscope, a confocal laser scanning microscope, and a transmission electron microscope. This study provided direct evidence that two morphologically distinct types of BM-derived cells were distributed in the mouse cornea. The majority of the GFP(+) cells showed a flattened polygonal form with obtuse angles and these cells were distributed in the corneal stroma. The other type was the GFP(+) cells demonstrating slim cell bodies with long and extremely thin dendrites and which were distributed in the corneal epithelium. The immunohistochemical characteristics and ultrastructure of BM-derived cells suggest that most of these cells have a macrophage lineage, whereas some cells in the corneal stroma do not. Interestingly, the direct intimate contact between GFP-labeled BM derived cells and non-GFP-labeled resident cells within the corneal stroma were also clearly visualized at the fine structural level. These data provide new and more detailed insight into the nature of BM-derived cells in the cornea. Anat Rec, 292:756–763, 2009.

Key words: cornea; bone marrow; green fluorescence protein; mouse

Grant sponsor: Ministry of Education, Culture, Sports, Science, and Technology, Japan; Grant number: 19791302.

*Correspondence to: Tetsuya Takayama, Division of Microscopic and Developmental Anatomy, Department of Anatomy, Kurume University School of Medicine, 67 Asahi-machi, Kurume, Fukuoka 830-0011, Japan. Fax: +81-942-31-7555.
E-mail: tetsuyataka@med.kurume-u.ac.jp

Received 2 August 2008; Accepted 23 December 2008
DOI 10.1002/ar.20851
Published online 18 February 2009 in Wiley InterScience (www.interscience.wiley.com).

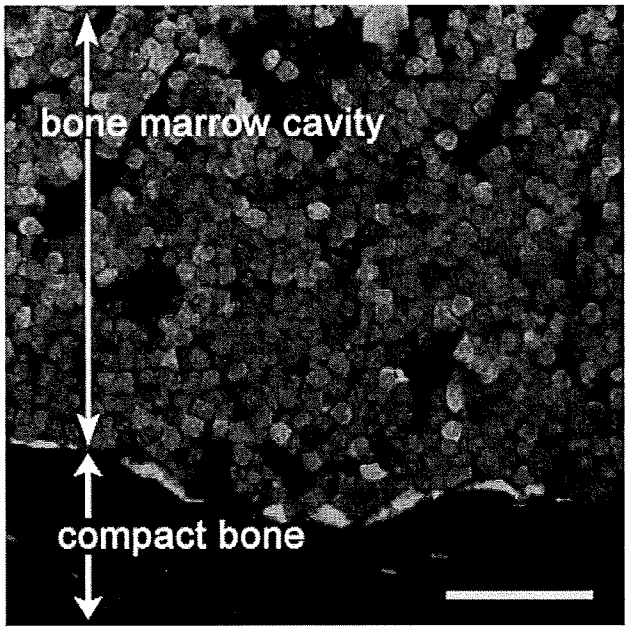

Fig. 1. Cross section of a femur of the BM reconstituted chimeric mouse. The BM cavity was almost completely occupied with green fluorescence of the transplants. The cell nuclei were stained with DAPI (blue). Scale bar = 50 μm.

Recently, particular attention has focused on the mesenchymal stem cells. These are multipotent cells present in bone marrow (BM) that can replicate as undifferentiated cells and have the potential to differentiate to lineages of mesenchymal tissues including bone, cartilage, fat, tendon, muscle, and marrow stroma (Prockop, 1997; Pittenger et al., 1999). These cells also can become neurons or cardiac muscle cells under specific conditions (Makino et al., 1999; Holden and Vogel, 2002; Jiang et al., 2002; Dezawa et al., 2004). These findings lead us to an idea that BM-derived stem cells may have the ability to transdifferentiate into a variety of cells in tissues, including those in the eye. Therefore, they may represent a renewable source of various cells in the human body, and harnessing their regenerative ability may aid in the treatment of various intractable degenerative diseases.

From an immunological viewpoint, the rejection of transplanted tissues or organs of the donor caused by the BM derived cells (e.g., antigen-presenting cells such as macrophages, dendritic cells, and B cells) of the recipient is assumed. The control of this immunoreaction is therefore closely related to the success or failure of the transplantation medicine. The cornea is located in the anterior segment of the eye and combines transparency and refractive ability for correct vision. Although the vascular system is required to provide the cells with a sufficient supply of nutrients in general, the cornea is a unique avascular tissue required for optical clarity and optimal vision. The nutritional requirements are derived from the tear film, the aqueous humor, and the limbal blood vessels. Therefore, the avascular central cornea has been thought to be an immune-privileged site without functional migrating cells which participate in the immune system (Streilein et al., 1979; Rowden, 1980; Peeler and Niederkorn, 1986) and assumed to be in an advantageous position for allografts in comparison with the other organs. Human corneal allografts really have achieved a high success rate in clinical medicine. However, recent reports showed a significant number of BM-derived antigen-presenting cells to be distributed in the cornea, based on indirect evidence obtained by immunohistochemical studies (Brissette-Storkus et al., 2002; Sosnova et al., 2005).

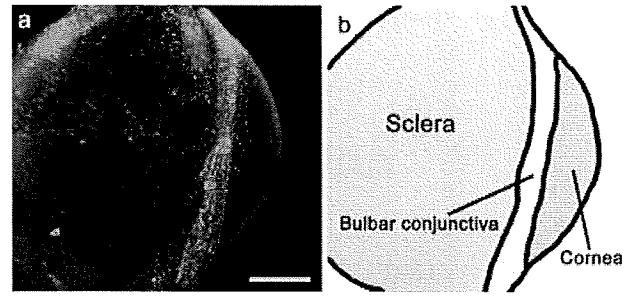

Fig. 2. (a) A fluorescent biomicroscopic image of an extracted eyeball from BM transplanted mouse. A large number of GFP(+) donor derived cells were noted as green dots which were scattered throughout the sclera and cornea. A part of the bulbar conjunctiva was also observed. Scale bar = 500 μm. (b) A schematic drawing of (a).

In the present study, enhanced green fluorescence protein (eGFP)-labeled BM cells were transplanted into syngeneic C57BL/6 (wild-type) mice to follow the fate of the BM-derived cells. The distribution pattern, immunohistochemical characteristics, three-dimensional structure, and the ultrastructure of the eGFP-labeled cells distributed in the cornea were investigated to obtain new and more detailed insight into their nature.

MATERIALS AND METHODS

Animals and BM Syngeneic Transplantation

The mice were treated in accordance with the ARVO Statement for the Use of Animals in Ophthalmic and Vision Research. Experiments were performed according to the guidelines established by the Institutional Animal Committee of Kurume University School of Medicine and Kyushu University.

Nonpurified BM cells harvested from femurs and tibiae of GFP transgenic mice at 8–12 weeks of age, were intravenously injected into wild-type C57BL/6 mice (N = 6) within 48 hr of birth after 400 cGy irradiation, as previously described (Hisatomi et al., 2003; Ishikawa et al., 2006). The GFP transgenic mice were C57BL/6 mice that transgenically express eGFP driven by the chicken beta actin promoter (Okabe et al., 1997; Ikawa et al., 1998) and purchased from Jackson Laboratory (Bar Harbor, ME). Four to six months after BM transplantation, the corneas of the chimeric mice were used for the histological and immunohistochemical studies. Age-matched untreated C57BL/6 mice (N = 6) were used as controls. All the mice were housed in 12-hr light:dark cycles and fed *ad libitum* with standard chow.

Fluorescence Microscopy

The mice were perfused transcardially with 4% paraformaldehyde in 0.1 M phosphate buffer (PB) under

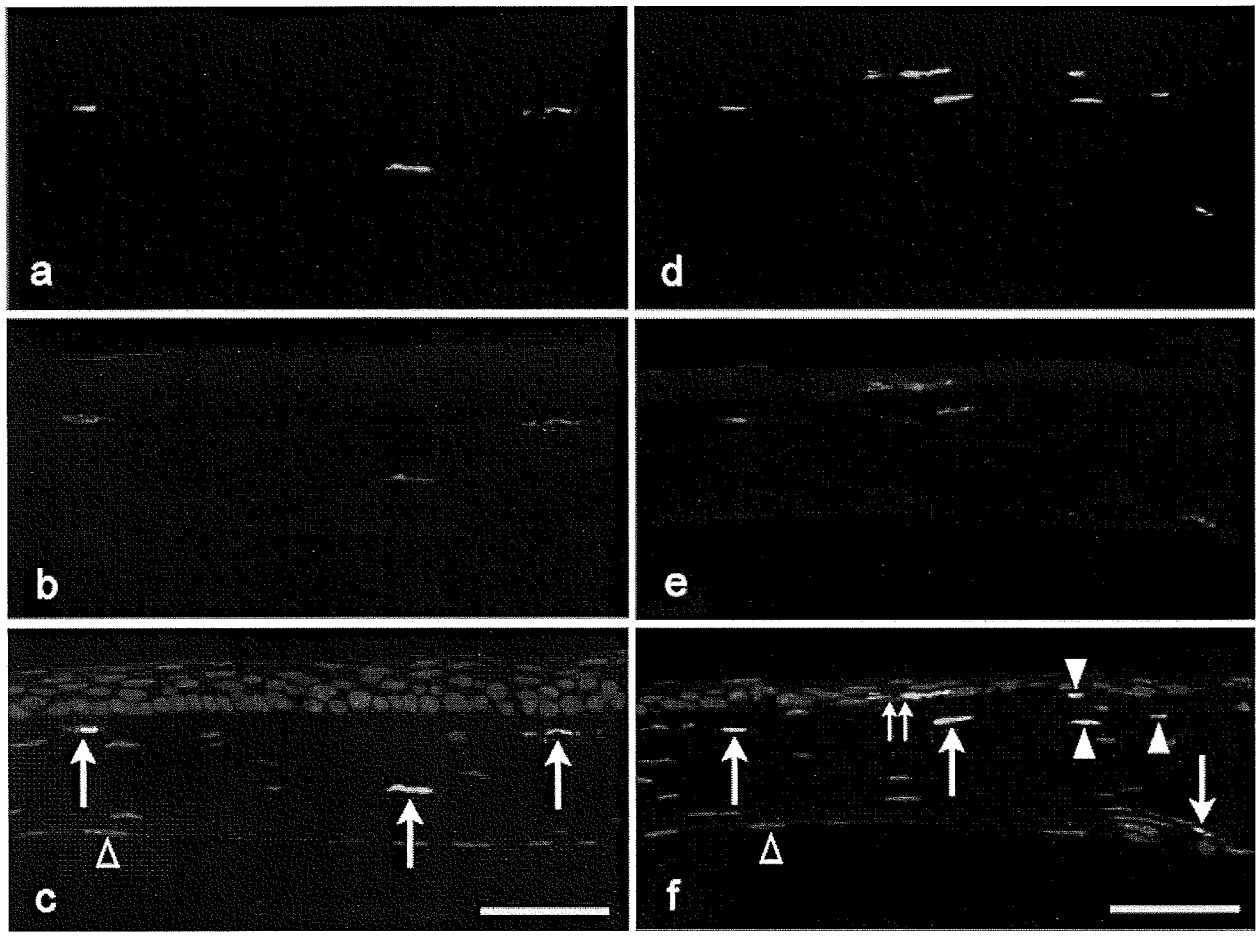

Fig. 3. Immunohistochemical staining for Iba1 (red) in the central (a–c) and peripheral (d–f) cornea of mice receiving BM transplants. (a–c) In the central cornea, a few GFP(+) cells (green) immunostained with Iba1 (arrows in c) were observed in the corneal stroma. (d–f) In the peripheral cornea, many GFP(+) cells were distributed in the corneal stroma. Though most of the GFP(+) cells were located in the corneal stroma and immunostained with Iba1 (arrows in f), they could only occasionally be found in the corneal epithelium (double small arrows in f). Note some GFP(+)Iba1(−) cells in the corneal stroma (arrowheads in f). Open arrowheads indicate the nuclei of the corneal endothelial cells (c, f). GFP (a, d), Iba1 (b, e), Overlap of GFP and Iba1 immunostaining (c, f). The cell nuclei were stained with DAPI (blue in c and f). Scale bars = 50 μm.

deep anesthesia with the intraperitoneal injection of Nembutal. The femurs and eyes were removed, and the eyes were observed under a fluorescent biomicroscopy (SMZ 1500; Nikon, Tokyo, Japan). After they were postfixed overnight with the same fixative, the corneas were removed from the eyes. Thereafter the femurs and corneas were washed and cryoprotected with 30% sucrose in PB, embedded in optimal cutting temperature (OCT) compound (Tissue-Tek; Sakura Finetechnical, Tokyo, Japan) and frozen in liquid nitrogen. Cryostat sections (10 μm in thickness) were placed on poly-L-lysine coated slides, air dried, and rehydrated in PB. Non-specific binding sites were blocked by 30-min incubation in PB containing 0.2% bovine serum albumin (BSA), 0.8% Gelatin and 0.2% Triton X-100 at room temperature. Thereafter, the sections were incubated overnight in the blocking solution described above with rabbit anti-Iba1 antibodies (Wako, Osaka, Japan) or purified hamster anti-mouse CD11c (BD Pharmingen, San Diego, CA) at 4°C. After several washes with PB, the sections were incubated at room temperature for 1 hr with the appropriate secondary antibodies, Alexa Fluor 568 goat anti-rabbit IgG(H+L) or Alexa Fluor 568 goat anti-hamster IgG(H+L) (Molecular Probes, Eugene, OR). After washed with PB, the cell nuclei were stained with DAPI (Dojin Chem, Kumamoto, Japan) and washed again. Coverslips were applied using mounting medium (PermaFluor Aqueous Mounting Medium; Pittsburgh, PA) and examined under a fluorescence microscope (Axioskop; Zeiss, Germany). All images were digitally acquired and recompiled (photoshop 5.0; Adobe, San Jose, CA). Immunohistochemical negative controls of the sections were performed by omitting the primary antibodies. These sections did not show any specific immunoreactivity. Only the cell nuclei were stained using DAPI in the femur sections and the immunohistochemical staining steps were omitted.

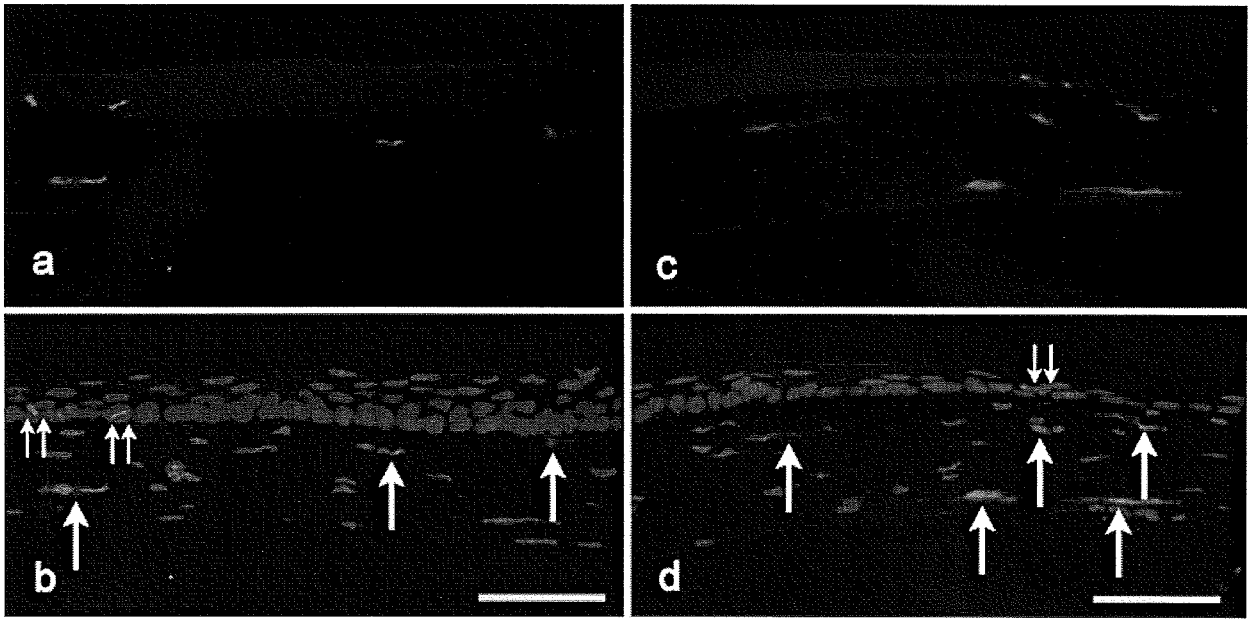

Fig. 4. Immunohistochemical staining for Iba1 (red) in the central (**a, b**) and peripheral (**c, d**) cornea of untreated wild mice. Most of the Iba1(+) cells were distributed in the corneal stroma (arrows), and their cell density was higher in the peripheral cornea in comparison to the central cornea. A few Iba1(+) cells were also noted in the corneal epithelium (double small arrows). The cell nuclei were stained with DAPI (blue in b and d). Scale bars = 50 μm.

Whole-Mount Corneas for Confocal Microscopy

The mice were perfused transcardially with 4% paraformaldehyde in PB under deep anesthesia, and the entire corneas were excised at the limbus under an operating microscope. Then they were postfixed with the same fixative overnight. After four radial cuts were performed by a sharp razor blade, the corneas were washed in PB. The cell nuclei were stained with DAPI and washed again. Coverslips were applied to the whole-mount corneas using mounting medium and they were examined with a laser scanning confocal microscope (Fluoview FV1000; Olympus, Tokyo, Japan). To acquire a three-dimensional image of the GFP(+) cells, multiple Z-sections were obtained through the entire corneal thickness (en face to the plane of the flattened cornea) and then a single image was created.

Immunoelectron Microscopy

Immunolabeling of the GFP(+) cells was performed using pre-embedding immunoelectron microscopy techniques. In brief, mice were perfused transcardially with 3.75% acrolein/2% paraformaldehyde in 0.1 M PB, followed with 4% paraformaldehyde in 0.1 M PB under deep anesthesia. The corneas were excised from the eyes and postfixed overnight with 4% paraformaldehyde in 0.1 M PB. Next, they were washed and cryoprotected with 30% sucrose in PB, embedded in OCT compound and frozen in liquid nitrogen. Vertical sections of the corneas were cut at 30 μm on a cryostat. The sections were washed in 0.1 M PB, immersed in 1% $NaBH_4$ in 0.1 M PB for 30 min. Thereafter, the sections were rinsed in 0.2% BSA/0.1 M tris buffered saline (TBS) for 1 hr. These sections were immersed in a blocking solution (0.1 M TBS containing 1% BSA, 0.8% Gelatin) for 1 hr, and then incubated for 2 days at 4°C with chicken anti-green fluorescent protein polyclonal antibody (Chemicon, Temecula, CA) diluted in the blocking solution described above. Thereafter, the sections were rinsed in 0.2% BSA/0.1 M TBS several times and incubated with biotin-SP-conjugated rabbit anti-chicken IgG (Chemicon). After further washes in 0.2% BSA/0.1 M TBS, the sections were preincubated for 4 hr in Strept ABC Working solution prepared according to the instructions included in the Streptavidin Biotin Complex Peroxidase kit (Nacalai Tesque, Kyoto, Japan). Subsequently, the sections were washed in 0.1 M PB, postfixed in 1% glutaraldehyde in 0.1 M PB for 10 min. After several washes in 0.1 M PB, they were incubated in the VIP solution which was prepared according to the instructions included in the Vector® VIP substrate kit for peroxidase (Vector Laboratories, Burlingame, CA). After several washings in 0.1 M PB, the sections were postfixed with 0.5% osmium tetroxide in 0.1 M PB for 30 min, dehydrated in a graded series of acetone solutions and flat-embedded in Epok 812 (Okenshoji, Tokyo, Japan). Ultrathin sections were stained with lead citrate, and then were photographed using a transmission electron microscope (H-7000; Hitachi, Tokyo, Japan). Control sections were processed the same way as described above, except that the first antibody was omitted, thus resulting in no specific staining.

RESULTS

Fluorescence Microscopy

Our observations of the cross-sections of the femurs confirmed that the BMs of the recipient mice were almost completely substituted by the GFP(+) transplant cells (Fig. 1).

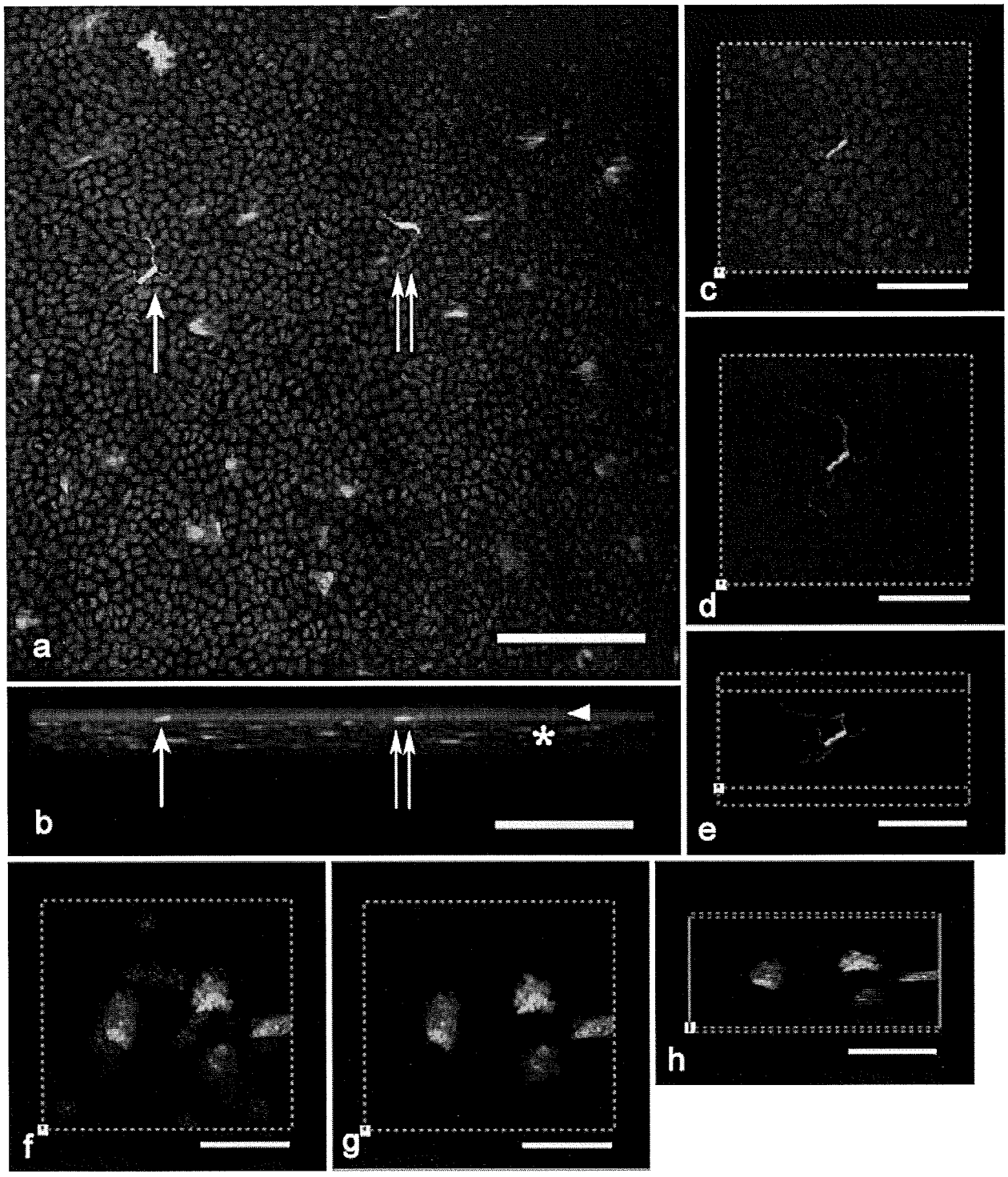

Fig. 5. Three-dimensional stereoscopic images of the whole-mount cornea preparations created with a confocal laser scanning microscope. The cell nuclei were stained with DAPI (blue) in (**a**–**c**) and (**f**). (a) Low-magnification photograph of the whole-mount preparation shows a lot of GFP(+) cells distributed in the cornea. (**b**) An image of a conventional cross section that inclined the image of (a) 90 degrees. The arrowhead and the asterisk indicate the corneal epithelium and the corneal stroma in each. Majority of the GFP(+) cells were distributed in the corneal stroma. A few GFP(+) cells observed in the corneal epithelium are indicated with an arrow or double arrows. These cells, which indicated with an arrow or double arrows in (b), correspond to the cells indicated with the same arrows in (a), respectively. (**c**–**h**) High-magnification images of the GFP(+) cells observed in corneal epithelium (c–**e**) and corneal stroma (f–h). (e) and (h) are the images that inclined the images of (**d**) and (**g**) 30 degrees to each. (c–e) In the corneal epithelium, GFP(+) cells which had slim cell bodies with a couple of long and extremely thin dendritic processes were observed. (f–h) In the corneal stroma, GFP(+) cells had the flattened polygonal form with obtuse angles. Scale bars = 100 μm for (a) and (b), 50 μm for (c–h).

Fluorescent biomicroscopical observations of the extracted eyeballs from the recipient mice revealed that a large number of GFP(+) donor derived cells were scattered throughout the sclera and cornea (Fig. 2). Vertical sections of the recipient corneas showed that the majority of the GFP(+) cells were distributed in the peripheral corneal stroma (Fig. 3d). On the other hand, a small number of the GFP(+) cells were observed in the central cornea (Fig. 3a). Though most GFP-labeled cells had thin typical spindle-shaped appearance and were localized to the corneal stroma, occasionally they could be found in the corneal epithelium (Fig. 3d–f). No GFP(+) cells were found in the corneal endothelium. In an immunohistochemical study, we used a macrophage marker Iba1 and a dendritic cell marker CD11c. Most of the GFP(+) cells were Iba1 positive, while some cells in the corneal stroma were not (Fig. 3c,f). Few CD11c(+) cells were observed in the cornea, and no GFP(+)CD11c(+) cells were detected (data not shown).

As a control study, the vertical sections of the untreated wild mouse corneas were also stained for Iba1. Most of the Iba1(+) cells were distributed in the corneal stroma, and their cell density was higher in the peripheral cornea (Fig.4c,d) in comparison to the central cornea (Fig. 4a,b). A few Iba1(+) cells were also noted in the corneal epithelium(Fig. 4a–d).

Confocal Microscopy of Corneal Whole Mount

Low-magnification images of the corneal whole-mount preparations showed numerous GFP(+) cells distributed in the cornea (Fig. 5a,b). The majority of those cells were distributed in the corneal stroma, and a few cells could be found in the corneal epithelium (Fig. 5a,b). Stereoscopic images of higher-magnification showed a distinctive morphology of the GFP(+) cells observed in the corneal epithelium and stroma, respectively. In the corneal epithelium, GFP(+) cells which had slim cell bodies with a couple of long and extremely thin dendritic processes were observed (Fig. 5c–e). In the corneal stroma, GFP(+) cells had a flattened polygonal form with obtuse angles (Fig. 5f–h).

Electron Microscopy

Electron micrographs showed the ultrastructure of the GFP(+) cells visualized with the electron-dense granular reaction product of VIP. In the corneal stroma, they had a slim spindle shape with numerous finger-shaped projections on the cell surface (Fig. 6a) and vacuoles filled with amorphous material in the cytoplasm (Fig. 6a, inset). Occasionally, some GFP(+) cells seemed to lie in intimate contact with GFP(−) fibroblast-like cells (Fig. 6b, inset). Such GFP(+) cells had a smooth cell surface and resembled keratocytes in shape (Fig. 6b).

A small number of GFP(+) cells with poor cytoplasm were seen in the basal-cell layer of the corneal epithelium (Fig. 7a). Occasionally, portions of thin cytoplasm, which seemed to be the dendrites, were observed between the corneal epithelial cells (Fig. 7b).

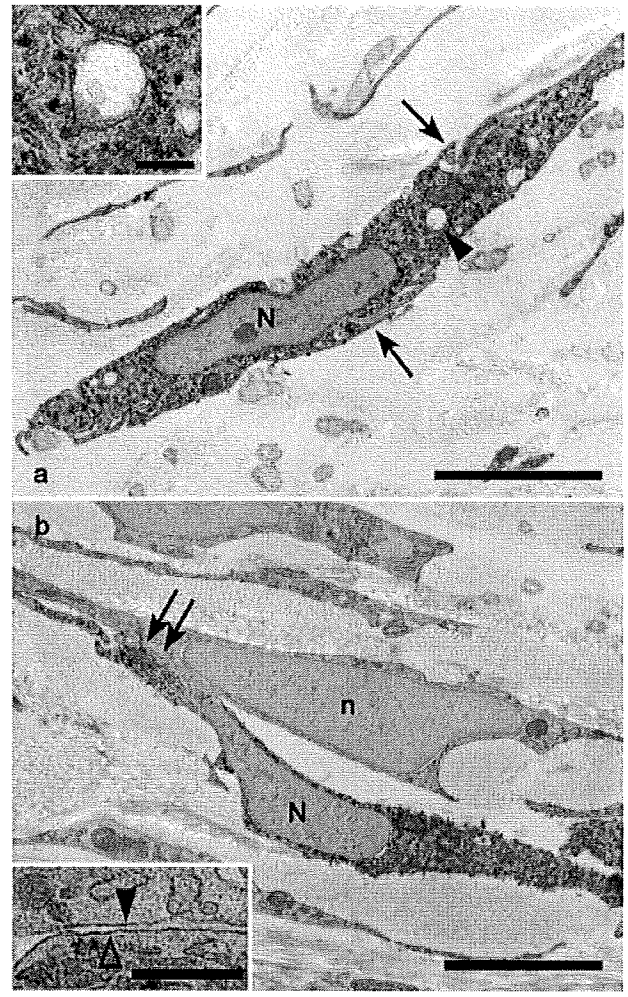

Fig. 6. Immunoelectron micrographs of the GFP(+) cells in the corneal stroma. Electron micrographs showing GFP (+) cells visualized with the electron-dense granular reaction product of VIP. (a) A GFP positive cell which had a spindle-shaped cell body and numerous finger-shaped projections on the cell surface (arrows). The inset, showing the area indicated by an arrowhead at higher magnification, reveals a vacuole filled with amorphous low-to-middle electron dense material. (b) A GFP(+) cell seemed to lie in intimate contact with a GFP(−) fibroblast-like cell. The inset, showing the area indicated by double arrows at higher magnification, reveals no specific intercellular junction. An arrow head, the position of the plasma membrane of a GFP(−) keratocyte; An open arrow head, the position of the plasma membrane of a GFP(+) cell; N, nuclei of GFP(+) cells; n, nucleus of GFP(−) cell. Scale bars = 3 μm in (a) and (b), 0.3 μm in the inset of (a), 0.5 μm in the inset of (b).

DISCUSSION

In the present study, we clearly demonstrated that at least two morphologically distinct forms of BM derived cells were distributed in the mouse cornea using a GFP-labeled BM transplantation chimeric mouse. Such direct visualization became possible only after the introduction of the present animal model.

Normal avascular corneal tissue consists of three cellular layers and two interfaces: the corneal epithelium, Bowman's layer, the stroma, Descemet's membrane, and the endothelium. The corneal epithelium is comprised of several layers of squamous epithelial cells overlying a

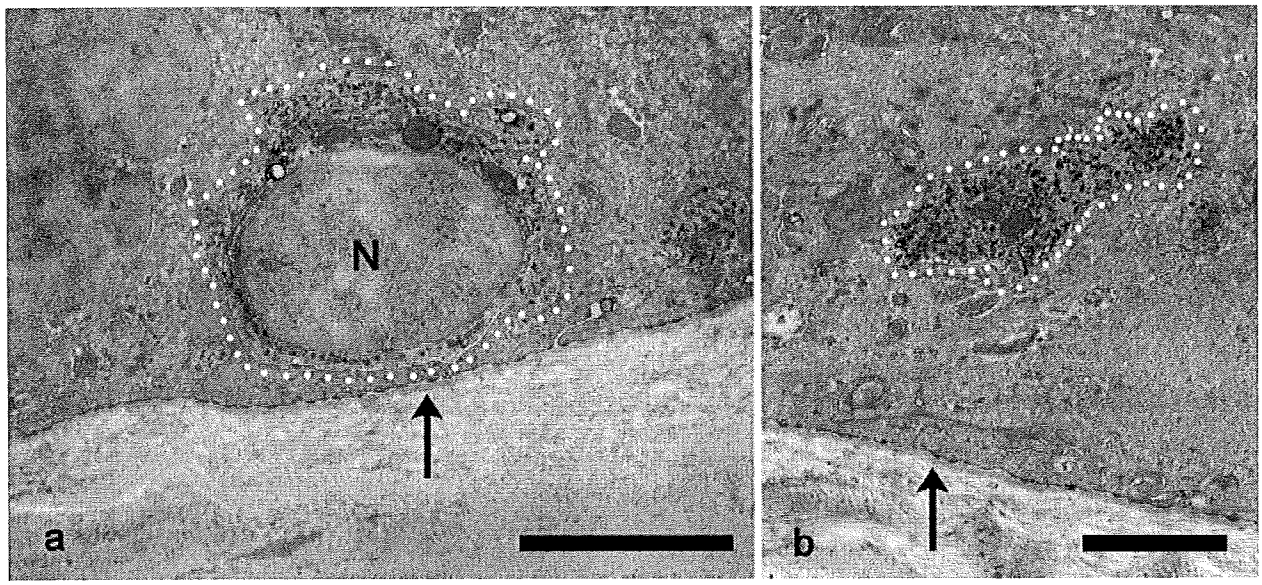

Fig. 7. Immunoelectron micrographs of the GFP(+) cells in the corneal epithelium. (**a**) A GFP(+) cell with poor cytoplasm located in the basal-cell layer of the corneal epithelium. (**b**) A portion which seemed to be a dendrite of the GFP(+) cell observed between the corneal epithelial cells. White dotted lines indicate GFP(+) cells and corneal epithelial cells borders. N, nucleus of GFP(+) cell; arrows, the position of the basal lamina. Scale bars = 3 μm in (a), 2 μm in (b).

layer of basal cells. The corneal stroma contains alternating lamellae of collagen fibrils and keratocytes (corneal fibroblasts), and the corneal endothelium is comprised of a single layer of polygonal cells. In vertical sections of the corneas of the chimeric mice, the majority of the GFP(+) cells were distributed in the corneal stroma between Bowman's layer and Descemet's membrane, and a small number were found in the corneal epithelium, which is above Bowman's layer.

The GFP(+) cells in the corneal epithelium and stroma were observed as slim spindle-shaped in the conventional vertical sections, and morphological heterogeneity was not distinguished under observations of fluorescence microscopy. As the GFP(+) cells are highly irregular in shape, it is hard for a whole cell body to be included in a cross-section of only 10 μm thick, thus making it difficult to obtain whole cell morphological images. Observations of the whole-mount preparations and confocal laser scanning microscopical recordings enable new dimensional analyses of those cells. Those revealed two characteristic stereoscopic structures of the GFP(+) cells depending on their respective localization patterns. In the corneal epithelium, GFP(+) cells had slim cell bodies with long and thin dendritic processes. On the other hand, in the corneal stroma, many GFP(+) cells had a flattened polygonal form with obtuse angles. Such a difference in the cell shapes might suggest the existence of subpopulations of BM derived cells in the cornea because BM essentially consists of a heterogeneous cell population. Their characteristic morphology may reflect each specific property, including potential functions. Another possibility is that BM derived cells are likely to change their form at will in order to adapt themselves to the circumferential microenvironment. GFP(+) cells in the corneal epithelium seemed to fit into the gap among the crowding cells, while their characteristic flattened shapes in the corneal stroma appeared to be ideal for existing among the lamellar structure of the stromal matrix consisting of dense collagen fascicles (Meek and Fullwood, 2001).

Electron microscopical observations demonstrated the detailed cytological features of the GFP(+) cells. Some GFP(+) cells in the corneal stroma showed the characteristic features of macrophages, such as finger-shaped projections on the cell surface, the absence of the basal lamina, and cytoplasmic vacuoles filled with amorphous material which were supposed to be lysosomes. Characteristic close contact between GFP(+) cells and GFP(−) keratocytes was occasionally observed in the present study. Previous studies of rat or rabbit cornea by transmission and scanning electron microscopy have shown the corneal keratocytes to be flattened, polygonal cells, and had cytoplasmic processes. The processes of neighboring keratocytes contacted each other to form an extensive and continuous network structure (Ueda et al., 1987; Nishida et al., 1988). These morphological characteristics of keratocytes closely resemble that of the GFP(+) cells observed in this study.

We observed more GFP(+) cells to be distributed in the peripheral part of cornea in comparison to the center of it, where the GFP(+) cell density was low. These findings may suggest that BM-derived cells migrated from the abundant blood vessels of the limbal vascular arcade which are distributed near the peripheral cornea, into the avascular central cornea. The self-renewal capacities of stromal keratocytes are poorly understood and the cell source is unclear so far. It is reported that BM-derived stem cells, such as hematopoietic and mesenchymal stem cells, have tremendous differentiation capacity beyond their blastoderm (Gussoni et al., 1999; Krause et al., 2001; Jiang et al., 2002). Taken together, the present findings raise the possibility that the stem cells from

the transplanted BM may transdifferentiate into corneal keratocytes and communicate with neighboring keratocytes, organizing themselves into a keratocyte cellular network in the corneal stroma. The GFP(+)Iba1(−) cells observed in the corneal stroma under a fluorescent microscope may represent such cells. On the other hand, it is reported that BM hematopoietic stem cells give rise to cardiomyocytes through cell fusion, not transdifferentiation (Ishikawa et al., 2006). We cannot exclude the possibility that BM-derived GFP(+) cells may fuse with resident corneal keratocytes. At any rate, further research is called to reveal the origin of such cells and clarify the biological significance of the intercellular close contact observed in this study.

It was recently reported that the normal corneal stroma contains a significant number of CD45+ leukocytes. Most these cells express the CD11b marker, but not other dendrite, granulocyte, T-cell, or NK markers, placing them in the monocyte/macrophage lineage (Brissette-Storkus et al., 2002). In the present study, most of the GFP(+) cells were immunostained for Iba1 which is a macrophage marker. In our control study, we also confirmed that Iba1(+) cells existed in the untreated wild mouse cornea in a distribution pattern similar to that of GFP(+) cells observed in BM chimeric mouse cornea. Such BM-derived macrophages may participate in various pathological responses and immunoinflammatory responses in the ocular anterior segment. On the other hand, some GFP(+) cells in the corneal stroma were not immunostained for Iba1 and their lineages were not determined. Some previous reports showed the existence of antigen presenting dendritic cells in normal murine and human cornea (Hamrah et al., 2003a,b; Nakamura et al., 2005; Yamagami et al., 2006). We failed to detect the signal of the dendritic cell marker CD11c. It was probably because the fixation method in this study was too strong to obtain an optimal signal for the CD11c antibody.

In summary, this study provides direct evidence that two morphologically distinct types of GFP-labeled BM-derived cells are distributed in the avascular cornea. We identified BM-derived cells which had slim cell bodies with long and thin dendrites in the corneal epithelium, and cells which showed a flattened polygonal form with obtuse angles in the corneal stroma. The immunohistochemical characteristics and ultrastructure of BM-derived cells suggest that most of these cells have a macrophage lineage, while some cells in the corneal stroma do not. This is a subject for future research to elucidate all lineages of bone marrow derived cells in cornea.

LITERATURE CITED

Brissette-Storkus CS, Reynolds SM, Lepisto AJ, Hendricks RL. 2002. Identification of a novel macrophage population in the normal mouse corneal stroma. Invest Ophthalmol Vis Sci 43:2264–2271.

Dezawa M, Kanno H, Hoshino M, Cho H, Matsumoto N, Itokazu Y, Tajima N, Yamada H, Sawada H, Ishikawa H, Mimura T, Kitada M, Suzuki Y, Ide C. 2004. Specific induction of neuronal cells from bone marrow stromal cells and application for autologous transplantation. J Clin Invest 113:1701–1710.

Gussoni E, Soneoka Y, Strickland CD, Buzney EA, Khan MK, Flint AF, Kunkel LM, Mulligan RC. 1999. Dystrophin expression in the mdx mouse restored by stem cell transplantation. Nature 401:390–394.

Hamrah P, Liu Y, Zhang Q, Dana MR. 2003a. The corneal stroma is endowed with a significant number of resident dendritic cells. Invest Ophthalmol Vis Sci 44:581–589.

Hamrah P, Liu Y, Zhang Q, Dana MR. 2003b. Alterations in corneal stromal dendritic cell phenotype and distribution in inflammation. Arch Ophthalmol 121:1132–1140.

Hisatomi T, Sakamoto T, Sonoda K, Tsutsumi C, Qiao H, Enaida H, Yamanaka I, Kubota T, Ishibashi T, Kura S, Susin SA, Kroemer G. 2003. Clearance of apoptotic photoreceptors: elimination of apoptotic debris into the subretinal space and macrophage-madiated phagocytosis via phosphatidylserine receptor and integrin alphavbeta3. Am J Pathol 162:1869–1879.

Holden C, Vogel G. 2002. Stem cells. Plasticity: time for a reappraisal? Science 296:2126–2129.

Ikawa M, Yamada S, Nakanishi T, Okabe M. 1998. 'Green mice' and their potential usage in biological research. FEBS Lett 430: 83–87.

Ishikawa F, Shimazu H, Shultz LD, Fukata M, Nakamura R, Lyons B, Shimoda K, Shimoda S, Kanemaru T, Nakamura K, Ito H, Kaji Y, Perry AC, Harada M. 2006. Purified human hematopoietic stem cells contribute to the generation of cardiomyocytes through cell fusion. FASEB J 20:E11–E17.

Jiang Y, Jahagirdar BN, Reinhardt RL, Schwartz RE, Keene CD, Ortiz-Gonzalez XR, Reyes M, Lenvik T, Lund T, Blackstad M, Du J, Aldrich S, Lisberg A, Low WC, Largaespada DA, Verfaillie CM. 2002. Pluripotency of mesenchymal stem cells derived from adult marrow. Nature 418:41–49.

Krause DS, Theise ND, Collector MI, Henegariu O, Hwang S, Gardner R, Neutzel S, Sharkis SJ. 2001. Multi-organ, multi-lineage engraftment by a single bone marrow-derived stem cell. Cell 105: 369–377.

Makino S, Fukuda K, Miyoshi S, Konishi F, Kodama H, Pan J, Sano M, Takahashi T, Hori S, Abe H, Hata J, Umezawa A, Ogawa S. 1999. Cardiomyocytes can be generated from marrow stromal cells in vitro. J Clin Invest 103:697–705.

Meek KM, Fullwood NJ. 2001. Corneal and scleral collagens: a microscopist's perspective. Micron 32:261–272.

Nakamura T, Ishikawa F, Sonoda K, Hisatomi T, Qiao H, Yamada J, Fukata M, Ishibashi T, Harada M, Kinoshita S. 2005. Characterization and distribution of bone marrow-derived cells in mouse cornea. Invest Ophthalmol Vis Sci 46:497–503.

Nishida T, Yasumoto K, Otori T, Desaki J. 1988. The network structure of corneal fibroblasts in the rat as revealed by scanning electron microscopy. Invest Ophthalmol Vis Sci 29:1887–1890.

Okabe M, Ikawa M, Kominami K, Nakanishi T, Nishimune Y. 1997. 'Green mice' as a source of ubiquitous green cells. FEBS Lett 407: 313–319.

Peeler JS, Niederkorn JY. 1986. Antigen presentation by Langerhans cells in vivo: donor-derived Ia^+ Langerhans cells are required for induction of delayed-type hypersensitivity but not for cytotoxic T lymphocyte responses to alloantigens. J Immunol 136:4362–4371.

Pittenger MF, Mackay AM, Beck SC, Jaiswal RK, Douglas R, Mosca JD, Moorman MA, Simonetti DW, Craig S, Marshak DR. 1999. Multilineage potential of adult human mesenchymal stem cells. Science 284:143–147.

Prockop DJ. 1997. Marrow stromal cells as stem cells for nonhematopoietic tissues. Science 276:71–74.

Rowden G. 1980. Expression of Ia antigens on Langerhans cells in mice, guinea pigs, and man. J Invest Dermatol 75:22–31.

Sosnova M, Bradl M, Forrester JV. 2005. $CD34^+$ corneal stromal cells are bone marrow-derived and express hemopoietic stem cell markers. Stem Cells 23:507–515.

Streilein JW, Toews GB, Bergstresser PR. 1979. Corneal allografts fail to express Ia antigens. Nature 282:326–327.

Ueda A, Nishida T, Otori T, Fujita H. 1987. Electron-microscopic studies on the presence of gap junctions between corneal fibroblasts in rabbits. Cell Tissue Res 249:473–475.

Yamagami S, Ebihara N, Usui T, Yokoo S, Amano S. 2006. Bone marrow-derived cells in normal human corneal stroma. Arch Ophthalmol 124:62–69.

Prostaglandin E receptor subtype EP3 in conjunctival epithelium regulates late-phase reaction of experimental allergic conjunctivitis

Mayumi Ueta, MD, PhD,[a,b] Toshiyuki Matsuoka, MD, PhD,[c] Shuh Narumiya, MD, PhD,[c] and Shigeru Kinoshita, MD, PhD[a] *Kyoto, Japan*

Background: We previously demonstrated that the prostaglandin E_2 (PGE_2)–EP3 pathway negatively regulates allergic reactions in a murine allergic asthma model.
Objectives: We investigated whether the PGE_2-EP3 pathway also regulates the development of murine experimental allergic conjunctivitis (EAC).
Methods: The expression of EP3 was examined by means of RT-PCR and immunohistochemistry in wild-type mice, as well as by means of 5-bromo-4-chloro-3-indolyl-β-D-galactopyranoside staining in mice deficient in *EP3* (*Ptger3*$^{-/-}$ mice) carrying the β-galactosidase gene at the *EP3* gene locus. EAC was induced by immunization of mice with short ragweed pollen (RW), followed by challenge with eye drops of RW, and eosinophil infiltration and *eotaxin-1* mRNA expression in the conjunctiva were examined. Mice were also treated with a topical application of an EP3-selective agonist during the elicitation phase. Quantitative RT-PCR was used to detect expression of *COXs* and *prostaglandin E synthases,* and ELISA was used to measure PGE_2 production in the eyelid.
Results: EP3 was constitutively expressed in conjunctival epithelium on the ocular surface. *Ptger3*$^{-/-}$ mice demonstrated significantly increased eosinophil infiltration in conjunctiva after RW challenge compared with wild-type mice. Consistently, significantly higher expression of *eotaxin-1* mRNA was observed in *Ptger3*$^{-/-}$ mice. Conversely, treatment of wild-type mice with an EP3-selective agonist resulted in a significant decrease in eosinophil infiltration, which was blunted in *Ptger3*$^{-/-}$ mice. Expression of *COX-2* and *prostaglandin E synthases* was upregulated and PGE_2 content was increased in the eyelids after RW challenge.
Conclusion: These data suggest that PGE_2 acts on EP3 in conjunctival epithelium and downregulates the progression of EAC. (J Allergy Clin Immunol 2009;123:466-71.)

Key words: Conjunctival epithelium, prostaglandin E receptor subtype EP3, allergic conjunctivitis, eosinophilic conjunctival inflammation, EP3 agonist

Allergy, especially type I allergy, such as asthma, allergic rhinitis, allergic conjunctivitis, allergic dermatitis, food allergy, and severe anaphylactic response, has increased enormously in prevalence during the past 2 decades[1] and has become one of the major health problems in our society. The course of allergic diseases can be divided into 2 phases: the early-phase reaction and the late-phase reaction. The early-phase reaction occurs within 1 hour after allergen exposure and is driven by the cross-linking of allergen-specific IgE bound to the high-affinity IgE receptor FcεRI on the surface of resident mast cells, the key effector cell in the early-phase reaction. The late-phase reaction occurs 12 to 24 hours after allergen challenge and is characterized by eosinophil-dominant inflammatory cell infiltration in which chemokines such as eotaxin play a key role.

Allergic conjunctivitis is ocular-surface inflammation associated with type I hypersensitivity reactions accompanied by the characteristic symptoms (itching, tearing, conjunctival edema, redness, and photophobia) during the early phase, and eosinophil infiltration occurs in conjunctivas during the late phase. The signs and symptoms of allergic conjunctivitis have a significant effect on patients' comfort, health, and quality of life. Patients with allergic conjunctivitis have a poor quality of life associated with their symptoms, and current treatments for allergic conjunctivitis are inadequate to cure them completely and sometimes lead to side effects, such as an increased risk for the development of cataracts and glaucoma caused by corticosteroids.[2] Therefore safer and more effective treatments are being sought.

One candidate for such treatment is the manipulation of prostanoids and their receptor-signaling pathways because they were reported to regulate allergic reactions in a mouse allergic asthma model. Although prostaglandin D_2 acts on its receptor, DP, and functions as a mediator of allergic asthma,[3] prostaglandin E_2 (PGE_2) acts on one of its 4 receptor subtypes, the prostaglandin E receptor subtype EP3, and negatively regulates allergic

From [a]the Department of Ophthalmology, Kyoto Prefectural University of Medicine; [b]the Research Center for Regenerative Medicine, Faculty of Life and Medical Sciences, Doshisha University, Kyoto; and [c]the Department of Pharmacology and Faculty of Medicine, Kyoto University.

Supported in part by grants-in-aid for scientific research from the Japanese Ministry of Health, Labour, and Welfare; the Japanese Ministry of Education, Culture, Sports, Science, and Technology; CREST from JST; the Kyoto Foundation for the Promotion of Medical Science; the National Institute of Biomedical Innovation of Japan; the Intramural Research Fund of Kyoto Prefectural University of Medicine; the Takeda Scientific Foundation; and the ONO Research Foundation. Financial relationship with manufacturer: We declare that the work described in the present paper was carried out in collaboration with Ono Pharmaceutical Co., Ltd., which supplied ONO-AE-248 used in this study and partially supported colonies of *Ptger3*$^{-/-}$ mice.
Disclosure of potential conflict of interest: S. Narumiya receives grant support from Ono Pharmaceuticals Co Ltd; the Ministry of Education, Culture, Sports, Science, and Technology of Japan; and the National Research of Biomedical Innovation, Japan; is a consultant for Zisai Research Institute; and is president of the Japanese Pharmacological Society. The rest of the authors have declared that they have no conflict of interest.
Received for publication June 27, 2008; revised September 22, 2008; accepted for publication September 29, 2008.
Available online November 11, 2008.
Reprint requests: Mayumi Ueta, MD, PhD, Department of Ophthalmology, Kyoto Prefectural University of Medicine, Kajiicho, Hirokoji, Kawaramachi, Kamigyoku, Kyoto 602-0841, Japan. E-mail: mueta@koto.kpu-m.ac.jp.
0091-6749/$36.00

doi:10.1016/j.jaci.2008.09.044